

Transport Properties of Anisotropic Polar Fluids: 1. Quadrupolar Interaction

G.A. Fernández, J. Vrabec^{*}, and H. Hasse

Institute of Thermodynamics and Thermal Process Engineering,
University of Stuttgart, D-70550 Stuttgart, Germany

Number of pages: 45

Number of tables: 1

Number of figures: 14

^{*} To whom correspondence should be addressed, tel.: +49-711/685-66107, fax: +49-711/685-66140, email: vrabec@itt.uni-stuttgart.de

ABSTRACT

Equilibrium molecular dynamics simulation and the Green-Kubo formalism were used to calculate self-diffusion coefficient, shear viscosity, and thermal conductivity for 30 different quadrupolar two-center Lennard-Jones fluids along the bubble line and in the homogeneous liquid. It was systematically investigated how anisotropy, i.e. elongation, and quadrupole momentum influence the transport properties. The reduced elongation L^* was varied from 0 to 0.8 and the reduced squared quadrupole momentum Q^{*2} from 0 to 4, i.e. in the entire range in which parameters for real fluids are expected. The statistical uncertainty of the reported data varies with transport property, for self-diffusion coefficient data the error bars are typically lower than 3%, for shear viscosity and thermal conductivity they are about 8 and 12%, respectively.

KEYWORDS: Green-Kubo; molecular dynamics; quadrupole; self-diffusion; shear viscosity; thermal conductivity.

1 INTRODUCTION

From the pioneering work of Alder et al. [1,2] who used molecular dynamics to investigate transport properties of hard-spheres, this method has proved to be a successful tool for the development and test of theories [3]; examples are the discovery of the hydrodynamic long-time tail [4] or the development of advanced kinetic theories [5,6]. Due to the increasing computer power, molecular dynamics is today an interesting option for studying [7] and predicting [8] transport properties. In particular, for predictions of transport properties of liquids, where no satisfactory analytical theory exists, molecular dynamics is the most suitable available method.

Molecular simulation is also attractive because it allows rigorous testing of theories and models, and systematically studying the influence of any molecular parameter on any transport property. Although real fluids usually consist of polar non-spherical molecules, most extensive studies on transport properties have been done on the basis of very simple molecular models, e.g. hard sphere potential [2,9], square well potential [10,11,12,13,14,15], steeply repulsive potential [16], or spherical Lennard-Jones potential [16,17].

In the present work, a systematic study on the influence of elongation and quadrupole momentum on self-diffusion coefficient, shear viscosity, and thermal conductivity of two-center Lennard-Jones plus point quadrupole (2CLJQ) fluids is carried out in the liquid region covering a broad range of temperature and density. This work is based on the knowledge of accurate vapor-liquid equilibria of 2CLJQ fluids from previous publications of Stoll et al. [18,19]. Molecular simulations are carried out along the bubble line and in the homo-

geneous liquid for different models over a grid of reduced temperatures and densities. Thus, a consistent comparison of the transport properties of different models is possible and subsequently the effect of elongation and quadrupole momentum can be identified.

It has been recently shown that the 2CLJQ model is not only an interesting model fluid but also suited for accurately describing the properties of real fluids. Vapor-liquid equilibria of 35 pure substances were successfully modeled with that approach [20,21]. Also for mixtures good results were achieved [19,22,23]. Furthermore, properties such as Joule-Thomson inversion [24], self-diffusion and binary Maxwell-Stefan diffusion coefficients [25], shear viscosity, and thermal conductivity [26] were reliably predicted by 2CLJQ models which were parameterized using vapor-liquid equilibrium data only.

2 MOLECULAR MODEL

The intermolecular interactions are represented by the two-center Lennard-Jones plus point quadrupole (2CLJQ) potential. The 2CLJQ potential is pairwise additive and consists out of two identical Lennard-Jones sites a distance L apart (2CLJ) plus a point quadrupole of momentum Q placed in the geometric center of the molecule oriented along the molecular axis connecting the two Lennard-Jones (LJ) sites. The interaction energy of two molecules i and j is given by

$$u_{ij}^{2CLJQ} = \sum_{a=1}^2 \sum_{b=1}^2 4\epsilon \left[\left(\frac{\sigma}{r_{ab}} \right)^{12} - \left(\frac{\sigma}{r_{ab}} \right)^6 \right] + u_Q. \quad (1)$$

Here, r_{ab} is one of the four LJ site-site distances; a counts the two LJ sites of

molecule i , b counts those of molecule j . The LJ parameters σ and ϵ represent size and energy, respectively. The contribution of a point quadrupole is given by [27]

$$u_Q = \frac{1}{4\pi\epsilon_0} \frac{3}{4} \frac{Q^2}{|\mathbf{r}_{ij}|^5} \left[1 - 5(c_i^2 + c_j^2) - 15c_i^2c_j^2 + 2(s_i s_j c - 4c_i c_j)^2 \right], \quad (2)$$

with $c_k = \cos\theta_k$, $s_k = \sin\theta_k$, and $c = \cos\phi_{ij}$. Herein, \mathbf{r}_{ij} is the center-center distance vector of two molecules i and j . θ_i is the angle between the axis of the molecule i and the center-center connection line and ϕ_{ij} is the azimuthal angle between the axis of molecules i and j . Finally, ϵ_0 is the electric constant in $8.854187817 \cdot 10^{-12} \text{ C}^2/(\text{J m})$.

A specific 2CLJQ model, e.g. for a real fluid like nitrogen, is fully determined by five parameters: σ , ϵ , L , Q [20,21] and the molecular mass m . But in molecular simulation all relevant physical properties can be treated in a reduced form. Here, they are related to σ , ϵ , and m , so that the reduced results are valid for all combinations of these three parameters. In this form, only two molecular parameters remain, i.e. reduced elongation $L^* = L/\sigma$ and reduced squared quadrupole momentum $Q^{*2} = Q^2/(4\pi\epsilon_0\epsilon\sigma^5)$. Henceforth, "squared" will be omitted in the text for brevity.

3 TRANSPORT COEFFICIENTS

Transport properties were calculated by equilibrium molecular dynamics simulation and the Green-Kubo formalism [28,29]. In this formalism, transport coefficients are obtained by integrating time autocorrelation functions of the corresponding microscopic fluxes.

The self-diffusion coefficient D is a measure for the mobility of individual molecules within a fluid. It is calculated by integration of the single molecule velocity autocorrelation function [30,31]

$$D = \frac{1}{3N} \int_0^\infty dt \langle \mathbf{v}_k(t) \cdot \mathbf{v}_k(0) \rangle, \quad (3)$$

where $\mathbf{v}_k(t)$ expresses the velocity vector of molecule k at some time t , and $\langle \dots \rangle$ denotes the ensemble average. Eq. (3) yields the self-diffusion coefficient averaging over N molecules.

The shear viscosity η , as defined in Newton's "law" of viscosity, describes the resistance of a fluid to shear forces. It refers to the resistance of an infinitesimal volume element to shear at constant volume [32]. The shear viscosity can also be related to momentum transport under the influence of velocity gradients. From a microscopic point of view, the shear viscosity can be calculated by integration of the time-autocorrelation function of the off-diagonal elements of the stress tensor, i.e. J_p^{xy} [30,31]

$$\eta = \frac{1}{Vk_B T} \int_0^\infty dt \langle J_p^{xy}(t) \cdot J_p^{xy}(0) \rangle, \quad (4)$$

where V is the molar volume, k_B is the Boltzmann constant, T the temperature, and $\langle \dots \rangle$ denotes the ensemble average. The statistics of the ensemble average in Eq. (4) can be improved using all three independent off-diagonal elements of the stress tensor, i.e. J_p^{xy} , J_p^{xz} , and J_p^{yz} . For a pure fluid, the component J_p^{xy} of the microscopic stress tensor \mathbf{J}_p is given by [33]

$$J_p^{xy} = \sum_{i=1}^N m v_i^x v_i^y - \frac{1}{2} \sum_{i=1}^N \sum_{j \neq i}^N \sum_{k=1}^3 \sum_{l=1}^3 r_{ij}^x \frac{\partial u_{ij}}{\partial r_{kl}^y}. \quad (5)$$

Here, i and j are the molecular indices. Lower indices l and k count all sites, including the quadrupolar site, and the upper indices x and y denote the vector component, e.g. for velocity v_i^x or center-center distance r_{ij}^x .

The thermal conductivity λ , as defined in Fourier's "law" of heat conduction, characterizes the capability of a substance for molecular transport of energy driven by temperature gradients. It can be calculated by integration of the time-autocorrelation function of the elements of the microscopic heat flow J_q^x and is given by [30,31]

$$\lambda = \frac{1}{Vk_B T^2} \int_0^\infty dt \langle J_q^x(t) \cdot J_q^x(0) \rangle. \quad (6)$$

The expression for the heat flow \mathbf{J}_q in pure fluids has been derived by Evans [33] and is given by

$$\mathbf{J}_q = \frac{1}{2} \sum_{i=1}^N \left((mv_i^2 + \mathbf{w}_i \mathbf{I}_i \mathbf{w}_i + \sum_{j \neq i}^N u_{ij}) \cdot \mathbf{v}_i \right) - \frac{1}{2} \sum_{i=1}^N \sum_{j \neq i}^N \sum_{k=1}^3 \sum_{l=1}^3 \mathbf{r}_{ij} \cdot \left(\mathbf{v}_i \frac{\partial u_{ij}}{\partial \mathbf{r}_{kl}} + \mathbf{w}_i \mathbf{\Gamma}_{ij} \right), \quad (7)$$

where \mathbf{w}_i is the angular velocity vector of molecule i , \mathbf{I}_i its matrix of angular momentum of inertia, and u_{ij} the intermolecular potential energy. The torque $\mathbf{\Gamma}_{ij}$ refers to a reference frame with origin in the molecular center of mass. As for shear viscosity, all three independent heat flow directions J_q^x , J_q^y , and J_q^z , can be used to improve the statistics of Eq. (6).

All results of this study were obtained and are presented in the reduced form, i.e. in relation to the molecular parameters size, energy, and mass. The reduced transport properties are defined by: $D^* = D/\sigma\sqrt{m/\epsilon}$, $\eta^* = \eta\sigma^2/\sqrt{m\epsilon}$, $\lambda^* = \lambda\sigma^2/k_B\sqrt{m/\epsilon}$. Relevant static thermodynamic properties, temperature $T^* =$

Tk_B/ϵ and number density $\rho^* = \rho\sigma^3$, are also reduced in the same sense. For the sake of brevity, "reduced" will be omitted in the following.

4 INVESTIGATED MODELS AND STATES

In the present work, 30 different model fluids were studied, where each fluid is fully determined by one combination of elongation L^* and quadrupole momentum Q^{*2} . Simulations at 16 liquid state points were carried out for each model fluid. In Figs. 1 and 2 four selected systems are shown; they illustrate the covered thermodynamic states and the influence of elongation and quadrupole momentum on the thermodynamic behavior of the fluids [18]. As Fig. 1 shows, critical temperature and density increase with increasing quadrupole momentum. On the other hand, Fig. 2 shows that these critical properties decrease with increasing elongation. Such a behavior can also be seen for linear Kihara fluids [34].

The studied model fluids have elongations that vary from $L^* = 0$, i.e. spherical molecules, to 0.8, i.e. strongly elongated dumbbell-shaped molecules, in six steps. The odd value $L^* = 0.505$ was chosen to cover the same model fluids as the previous work on vapor-liquid equilibria [18]. Five quadrupole momenta were studied that range from $Q^{*2} = 0$ to 4 with increments of unity. The upper limit of 4 is sufficient to describe strongly quadrupolar real fluids, eg. CO_2 with $Q = -3.7938 \text{ D}\text{\AA}$ ($Q^{*2} = 3.3037$), C_2H_2 with $Q = 5.0730 \text{ D}\text{\AA}$ ($Q^{*2} = 4$), or C_2F_4 with $Q = -7.0332 \text{ D}\text{\AA}$ ($Q^{*2} = 3.9272$) [20].

For the sake of consistency, transport properties for spherical fluids ($L^*=0$) were treated as two superimposed Lennard-Jones sites. This implies, that the

temperature has to be divided by 4 as well as the quadrupole momentum, if a direct comparison with a one-center Lennard-Jones fluid is to be made. The corresponding conversion of D^* , η^* , and λ^* for these spherical fluids is obtained dividing the present data by 2.

As temperatures and number densities in vapor-liquid equilibrium vary strongly with the molecular parameters, it is useful to introduce another reduced form for representing the temperature $T_R=T^*/T_c^*$ and the density $\rho_R=\rho^*/\rho_c^*$. Here, T_c^* is the critical temperature and ρ_c^* the critical density of the individual 2CLJQ fluid; values for T_c^* and ρ_c^* were taken from [18]. For each fluid, the considered reduced temperatures along the bubble line range from $T_R=0.6$ to 0.9 with increments of $\Delta T_R=0.1$. In addition to those four points, another 12 points in the homogeneous liquid region were simulated, cf. Figs. 1 and 2. These points were selected on isochores starting from each bubble point with temperature increments of $\Delta T_R=0.1$. In this way, also isothermal data was generated.

5 SIMULATION DETAILS

Equilibrium molecular dynamics simulations were performed in a cubic box of volume V containing $N = 500$ molecules. The cut-off radius was set to $r_c = 5\sigma$, otherwise to half of the box length. The molecules in the fluid were assumed to have no preferential relative orientations outside of the cut-off sphere. For the calculation of the LJ long range corrections, orientational averaging was done with equally weighted relative orientations as proposed by Lustig [35]. The assumption of no preferential relative orientations beyond the cut-off sphere implies that no long range corrections for the quadrupolar

interactions are needed since they disappear. This is a reasonable assumption as demonstrated by Streett and Tildesley [36]. The simulations were started with the molecules in a face centered cubic lattice with random velocities, the total momentum of the system was set to zero, and Newton's equations of motion were solved with the Gear predictor-corrector integration scheme of fifth order [37]. The time step for this algorithm was set to $\Delta t \sqrt{\epsilon/m}/\sigma = 0.0005$. Self-diffusion coefficient, shear viscosity, and thermal conductivity were calculated in the microcanonical NVE ensemble using Eqs. (3) to (7). The simulations were equilibrated in the canonical NVT ensemble between 100 000 to 150 000 time steps. After equilibration, the thermostat was turned off and the simulation continued in the NVE ensemble where the transport properties were calculated. Because of the lack of a thermostat, the temperature was fluctuating with a maximum drift of 3 %.

Statistical uncertainties were estimated using the standard deviation of four independent simulations of 3 000 independent autocorrelation functions. In order to achieve independence between autocorrelation functions, a time span of 0.1 in reduced units was left between consecutive autocorrelation functions. This time span was consistent with a decay to less than $1/e$ of the normalized velocity autocorrelation function in several pilot runs. It is a conservative choice, when a compromise between simulation time and accuracy has to be done. Fig. 3 shows the normalized autocorrelation functions (ACF) from top to bottom for self-diffusion coefficient, shear viscosity, and thermal conductivity for the 2CLJQ fluid with $L^*=0.2$ and $Q^{*2}=1$ for the bubble point at 70 % of its critical temperature ($T_c^* = 4.388$), where the bubble density is $\rho^* = 0.6573$. The vertical line denotes $t^*=0.1$, the horizontal line the value $1/e$. All three ACF fulfill the criterion of independence between consecutive correlations,

although they show a quite different decay. Another important issue is the significant length of the autocorrelation functions, or equivalently, how long they must be integrated. Fig. 4 shows the integrals from top to bottom for self-diffusion coefficient, shear viscosity, and thermal conductivity. In principle, the integration of the ACF must be carried out until the integral shows stationary behavior. In practice, the convergence of the self-diffusion integral is difficult to guarantee for all conditions, because of the long time behavior [4] with a decay proportional to $t^{3/2}$. A similar problem is present regarding the autocorrelation function for shear viscosity close to the fluid-solid transition [2,38,39,40]. Here it was handled by a long evaluation ($\Delta t^* = 1.25$) of the ACF, as can be seen in Fig. 4. The integrals converge to the final value at around 0.5, afterwards the ACF fluctuate around zero, cf. Fig. 3, without effective contribution to the integrals.

6 RESULTS

In this section, the simulation results for the transport coefficients are presented. Numerical data for self-diffusion coefficient, shear viscosity, and thermal conductivity are given in Table I for elongations from $L^*=0$ to 0.8 and quadrupole momenta from $Q^{*2}=0$ to 4. All data in Table I correspond to state points along the bubble line for reduced temperatures of $T_R=0.6, 0.7, 0.8,$ and 0.9 . The complete data set, with 12 additional state points in the liquid region for each fluid, is available in [41] and partially included in Figs. 7, 8, 10, 11, 13, and 14. The effects of elongation, quadrupole momentum, temperature, and density are discussed in the following for each transport coefficient separately.

The accuracy of the calculated transport properties decreases in the sequence

self-diffusion coefficient, shear viscosity, thermal conductivity. The high accuracy of the self-diffusion coefficient, with error bars lower than 3 %, is due to its individual nature [3]. Shear viscosity and thermal conductivity are collective properties, consequently they show for the same simulation time and system size larger uncertainties, that are around 8 and 12 %, respectively. In most simulations of the present work the autocorrelation functions of thermal conductivity decay faster than those for shear viscosity, but fluctuate more. Figs. 3 and 4 illustrate this.

Other factors that influence the accuracy of the reported data are elongation and quadrupole momentum. In particular, at low temperatures, for fluids with large anisotropy and strong quadrupole momentum, the transport coefficients show larger simulation uncertainties.

In the following, the results are discussed for nine selected fluids, covering the whole range of the two molecular parameters, from spherical ($L^*=0$) over elongated ($L^*=0.505$) to strongly elongated ($L^*=0.8$) fluids with varying quadrupole momentum of $Q^{*2}=0, 2$, and 4 . A subset of six fluids is taken in some cases only due to graphical reasons.

6.1 *Self-diffusion coefficient*

Figs. 5 and 6 illustrate the self-diffusion coefficient along the bubble line for nine selected fluids. The results can either be discussed in terms of reduced density ρ_R as in Fig. 5 or in terms of number density ρ^* as in Fig. 6. From Fig. 5 it can be seen that the regarded range of reduced density is similar for all fluids, but significant deviations from the principle of corresponding states are

present also for the density. At constant T_R , it can be discerned that the self-diffusion coefficient decreases with both increasing elongation and quadrupole momentum. A better visibility of the data (which is even more needed for the less accurate properties shear viscosity and thermal conductivity) is obtained when plotted over number density in Fig. 6. Therefore, this graphical representation is preferred in the following.

As Fig. 6 shows, D^* decreases with increasing number density along the bubble line (where with increasing density also the temperature decreases). It is an important result of the present study that the self-diffusion coefficient lies roughly along the same line for a given elongation, independent of the quadrupole momentum.

Fig. 7 shows the dependence of D^* on number density in the homogeneous liquid region at a constant reduced temperature of $T_R=0.9$. Note that the density range is the same as in Fig. 6. Along this isotherm D^* decreases slightly hyperbolic with increasing density, resembling the behavior of D^* along bubble lines for a given elongation. Comparing D^* along bubble lines with isothermal data for an identical density variation, it is found that the density effect dominates with a contribution of 80 %.

Fig. 8 shows the dependence of the self-diffusion coefficient on temperature at different constant densities for a subset of six fluids. The isochores correspond to bubble densities at the reduced temperature $T_R=0.6$, cf. Figs. 1 and 2, which have similar values in terms of ρ_R . Along the isochores, the self-diffusion coefficient increases linearly with increasing temperature. The gradients with respect to reduced temperature are almost constant for a given elongation, where the slope is less steep for more elongated fluids. Such a linear dependence

of D^* on temperature has also been reported by other authors for Lennard-Jones fluids [42], Kihara fluids [7], and two-center Lennard-Jones fluids [43].

6.2 Shear viscosity

Fig. 9 illustrates the shear viscosity along the bubble line for the nine selected fluids. At constant T_R , it is found that the shear viscosity decreases with increasing elongation but increases with increasing quadrupole momentum. Again it is found that the results for a given elongation lie roughly along one line independent of Q^{*2} , where, as expected, they increase with increasing number density.

The density dependence of shear viscosity in the homogeneous liquid region is illustrated in Fig. 10 at $T_R=0.9$. Comparing the variation of η^* along bubble lines and along isotherms in the same way as for D^* , it is found for non-polar fluids that the density effect is responsible for about 80 % of the increase of η^* along the bubble line. For quadrupolar fluids, however, the temperature influence becomes more important and its contribution is about 40 %.

Fig. 11 shows the dependence of shear viscosity on reduced temperature for a subset of six fluids along isochores with similar values in terms of ρ_R . As expected, shear viscosity decreases with increasing temperature. Strongly quadrupolar fluids, with an about threefold higher shear viscosity in the cold liquid, are more sensitive to temperature, exhibiting larger gradients.

6.3 Thermal conductivity

Fig. 12 illustrates the thermal conductivity along the bubble line. Again, the data lie roughly along single lines for a given elongation, but considering simulation uncertainties not more than a linear dependence can be discerned. Thermal conductivity has the same basic trends like shear viscosity as it decreases with increasing elongation but increases with increasing quadrupole momentum at constant T_R .

Fig. 13 shows the density dependence in the homogeneous liquid at $T_R=0.9$. It can be seen that the curves resemble those along bubble lines, underlining the dominating effect of density there. Similar results have been reported by Tokumasu et al. [44] who studied the non-polar 2CLJ potential but at different thermodynamic conditions. In their analysis, Tokumasu et al. reduced λ^* by critical temperature and critical density, to isolate the effect of elongation and found that this type of reduced thermal conductivity increases with increasing elongation.

Fig. 14 shows isochoric data with similar values in terms of ρ_R for a subset of six fluids, where the effect of temperature on λ^* is small. Taking the statistical uncertainty and the scatter into account, hardly any trend can be discerned. Experimental results [45,46] show that thermal conductivity at constant density increases with increasing temperature, but the variation is very small in the liquid region. Moreover, the increase of λ^* with increasing quadrupole momentum can be seen.

7 CONCLUSION

Equilibrium molecular dynamics simulation and the Green-Kubo formalism were used to calculate self-diffusion coefficient, shear viscosity, and thermal conductivity for 30 different anisotropic and quadrupolar model fluids. A comprehensive data set was obtained for each fluid and property that covers a substantial part of the liquid state. The statistical uncertainty of the reported data varies according to transport property. For self-diffusion coefficient data, it is less than 3 %, for shear viscosity and thermal conductivity it is around 8 and 12 %, respectively.

The three transport properties are dominated in the investigated liquid region by the density: saturated liquid and isothermal data for fluids with a given elongation but varying quadrupole momentum lie roughly along single lines when plotted over number density.

However, all transport properties on the bubble line at a constant reduced temperature are lower for fluids with larger elongation. An increasing quadrupole momentum also leads to a lower self-diffusion coefficient, the opposite is found for shear viscosity and thermal conductivity.

Temperature influences all transport properties less than density. As expected, along isochores, the self-diffusion coefficient increases with temperature, the shear viscosity decreases, and for the thermal conductivity hardly any variation can be discerned.

List of symbols

a	interaction site index
b	interaction site index
c	short notation for a trigonometric function
D	self-diffusion coefficient
i	molecule index
j	molecule index
J_p	element of the microscopic stress tensor
J_q	element of the microscopic heat flow
k	interaction site index
k	molecule index
k_B	Boltzmann constant
l	interaction site index
L	molecular elongation
m	molecular mass
N	number of molecules
Q	molecular quadrupole momentum
r	site-site distance
r_c	center-center cut-off radius
s	short notation for a trigonometric function
t	time
T	temperature
u	pair potential
v	element of the velocity vector
V	molar volume
Δ	increment
Δt	integration time step
ϵ	Lennard-Jones energy parameter
ϵ_0	Electric constant

η shear viscosity
 θ angle of nutation
 λ thermal conductivity
 ρ density
 σ Lennard-Jones size parameter
 ϕ azimuthal angle

Vector properties

\mathbf{I} matrix of angular momentum of inertia
 \mathbf{J}_p microscopic stress tensor
 \mathbf{J}_q microscopic heat flow vector
 \mathbf{r} distance vector
 \mathbf{v} velocity vector
 \mathbf{w} angular velocity vector
 $\mathbf{\Gamma}$ torque vector

Subscript

a interaction site index
 b interaction site index
 c property at critical point
 i molecule index
 j molecule index
 Q point quadrupole
 R property reduced by critical value
2CLJQ two-center Lennard-Jones plus point quadrupole

Superscript

x cartesian direction
 y cartesian direction
 z cartesian direction
* property reduced by molecular parameters

Acknowledgement

We gratefully acknowledge financial support from Deutscher Akademischer Austauschdienst (DAAD).

References

- [1] B.J. Alder, D.M. Gass, and T.E. Wainwright, *Phys. Rev. Lett.* **18** (1967) 988-990.
- [2] B.J. Alder, D.M. Gass, and T.E. Wainwright, *J. Chem. Phys.* **53** (1970) 3813-3825.
- [3] J.P. Hansen and I.A. McDonald, *Theory of Simple Liquids*, Academic Press, London, 1986.
- [4] B.J. Alder, in C. Ciccotti, and W.G. Hoover (Eds.) , *Molecular-dynamic simulation of statistical-mechanical systems*, North-Holland, Amsterdam, 1986, pp. 66-76.
- [5] P.M. Furtado, G.F. Mazenko, and S. Yip, *Phys. Rev. A* **14** (1976) 1641-1644.
- [6] T. Keyes and A.J. Masters, *Adv. Chem. Phys.* **58** (1985) 1-53.
- [7] L.G. MacDowell, B. Garzon, S. Calero, and S. Lago, *J. Chem. Phys.* **106** (1997) 4753-4767.
- [8] C. McCabe, C.W. Manke, and P.T. Cummings, *J. Chem. Phys.* **116** (2002) 3339-3342.
- [9] J.J. Erpenbeck and W.W. Wood, *J. Stat. Phys.* **24** (1981) 455-468.
- [10] J.P.J. Michels and N.J. Trappeniers, *Chem. Phys. Lett.* **66** (1979) 20-23.
- [11] J.P.J. Michels and N.J. Trappeniers, *Physica A* **101** (1980) 156-166.
- [12] J.P.J. Michels and N.J. Trappeniers, *Physica A* **104** (1980) 243-254.
- [13] J.P.J. Michels and N.J. Trappeniers, *Physica A* **107** (1981) 158-165.
- [14] J.P.J. Michels and N.J. Trappeniers, *Physica A* **107** (1981) 299-306.
- [15] J.P.J. Michels and N.J. Trappeniers, *Physica A* **116** (1982) 516-525.
- [16] D.M. Heyes, *J. Phys. Condes. Matter.* **6** (1994) 6409-6421.
- [17] D.M. Heyes, *J. Chem. Phys. Faraday Trans.* **79** (1983) 1741-1758.
- [18] J. Stoll, J. Vrabec, H. Hasse, and J. Fischer, *Fluid Phase Equilib.* **179** (2001) 339-362.
- [19] J. Stoll, PhD Thesis, *Molecular models for the prediction of thermophysical properties of pure fluid and mixtures*, Reihe 3, Band 836, VDI, Düsseldorf, 2005.
- [20] J. Vrabec, J. Stoll, and H. Hasse, *J. Phys. Chem. B* **105** (2001) 12126-12133.
- [21] J. Stoll, J. Vrabec, and H. Hasse, *J. Phys. Chem.* **119** (2003) 11396-11407.
- [22] J. Vrabec, J. Stoll, and H. Hasse, *Mol. Sim.* **31** (2005) 215-221.

- [23] J. Stoll, J. Vrabec, and H. Hasse, *AIChE J.* **49** (2003) 2187-2198.
- [24] J. Vrabec, G.K. Kedia, and H. Hasse, *Cryogenics* **45** (2005) 253-258.
- [25] G.A. Fernández, J. Vrabec, and H. Hasse, *Int. J. Thermophys.* **26** (2005) 1389-1407.
- [26] G.A. Fernández, J. Vrabec, and H. Hasse, *Mol. Sim.* **31** (2005) 787-793.
- [27] C.G. Gray and K.E. Gubbins, *Theory of molecular fluids, Vol. 1, Fundamentals*, Clarendon Press, Oxford, 1984.
- [28] M.S. Green, *J. Chem. Phys.* **22** (1954) 398-413.
- [29] R. Kubo, *J. Phys. Soc. Jpn.* **12** (1957) 570-586.
- [30] K.E. Gubbins, in K. Singer (Eds.) , *Statistical mechanics vol. 1, The chemical society*, Burlington house, London, 1972.
- [31] W.A. Steele, in H.J.M. Hanley, (Eds.) , *Transport phenomena in fluids*, Marcel Dekker, New York and London, 1969.
- [32] A.F.M. Baron, *The dynamic liquid state*, Longman, London, 1974.
- [33] D.J. Evans and W.B. Streett, *Mol. Phys.* **36** (1978) 161-176.
- [34] C. Vega, S. Lago, E. de Miguel, and L.F. Rull, *J. Phys. Chem.* **96** (1992) 7431-7437.
- [35] R. Lustig, *Mol. Phys.* **65** (1988) 175-179.
- [36] W.B. Streett and D.J. Tildesley, *Proc. R. Soc. A* **355** (1977) 239-266.
- [37] J.M. Haile, *Molecular Dynamics Simulation*, John Wiley & Sons, New York, 1997.
- [38] D. Levesque, L. Verlet, and J. Kürkijarvi, *Phys. Rev. A* **7** (1973) 1690-1700.
- [39] M. Schoen and C. Hoheisel, *Mol. Phys.* **56** (1985) 653-672.
- [40] J.J. Erpenbeck, *Phys. Rev. A* **2** (1974) 2514-2528.
- [41] G.A. Fernández, *Transport properties of polar fluids by molecular simulation*, PhD Thesis, University of Stuttgart, 2006.
- [42] D. Levesque and L. Verlet, *Phys. Rev. A* **2** (1970) 2514-2528.
- [43] K. Singer, J.V.L. Singer, and A.J. Taylor, *Mol. Phys.* **37** (1979) 1239-1262.
- [44] T. Tokumasu, T. Ohara, and K. Kamijo, *J. Chem. Phys.* **118** (2003) 3677-3685.
- [45] V.P. Slyusar, V.M. Tretyakov, and N.S. Rudenko, *Sov. J. Low. Tem. Phys.* **1** (1975) 556-561.
- [46] V.P. Slyusar, V.M. Tretyakov, and N.S. Rudenko, *Sov. J. Low. Tem. Phys.* **4** (1978) 363-368.

Table I

Transport coefficients along the bubble line for 30 2CLJQ fluids of different elongation L^* and quadrupole momentum Q^{*2} . The numbers in parentheses denote the uncertainty in the last digits.

$L^*=0$	T^*	ρ^*	D^*	η^*	λ^*
$Q^{*2}=0$	3.156	0.8062	0.095(2)	4.83(9)	13.4(6)
	3.681	0.7453	0.155(4)	3.00(35)	11.0(13)
	4.255	0.6735	0.250(6)	2.00(24)	8.65(77)
	4.674	0.5838	0.388(5)	1.52(16)	6.37(51)
$Q^{*2}=1$	3.132	0.8201	0.080(1)	5.31(35)	11.7(12)
	3.712	0.7575	0.143(2)	3.62(23)	11.2(12)
	4.187	0.6851	0.228(4)	2.26(18)	9.8(12)
	4.773	0.5934	0.368(2)	1.58(6)	6.44(78)
$Q^{*2}=2$	3.398	0.8483	0.062(3)	7.67(46)	13.0(19)
	3.925	0.7819	0.119(1)	4.45(34)	10.7(22)
	4.538	0.7041	0.205(2)	2.64(25)	10.32(82)
	4.946	0.6055	0.339(3)	1.79(16)	7.07(11)
$Q^{*2}=3$	3.505	0.8796	0.047(1)	9.70(64)	15.4(25)
	4.106	0.8099	0.099(2)	5.83(58)	12.4(13)
	4.741	0.7292	0.179(1)	3.28(62)	10.4(19)
	5.341	0.6272	0.310(4)	1.93(26)	7.9(12)
$Q^{*2}=4$	3.841	0.9143	0.038(1)	14.02(86)	18.3(19)
	4.476	0.8430	0.081(1)	6.87(64)	15.9(17)
	5.164	0.7609	0.153(3)	3.85(21)	11.9(14)
	5.742	0.6579	0.275(4)	2.54(27)	9.8(15)

Table I
Continued.

$L^*=0.2$	T^*	ρ^*	D^*	η^*	λ^*
$Q^{*2}=0$	2.589	0.7114	0.089(1)	3.64(16)	11.58(59)
	3.015	0.6573	0.147(1)	2.63(7)	9.69(74)
	3.441	0.5946	0.228(6)	1.74(11)	7.67(83)
	3.874	0.5144	0.353(7)	1.27(5)	5.90(30)
$Q^{*2}=1$	2.625	0.7203	0.083(1)	4.19(21)	12.1(10)
	3.070	0.6644	0.142(2)	2.86(23)	11.7(13)
	3.496	0.5998	0.226(4)	1.89(9)	8.54(57)
	3.941	0.5185	0.350(9)	1.19(7)	6.74(28)
$Q^{*2}=2$	2.722	0.7420	0.075(1)	4.78(36)	17.1(14)
	3.195	0.6833	0.133(2)	2.97(12)	15.4(15)
	3.659	0.6167	0.215(4)	2.12(14)	11.76(93)
	4.072	0.5322	0.338(8)	1.34(8)	7.74(47)
$Q^{*2}=3$	2.877	0.7683	0.067(1)	5.48(21)	21.0(29)
	3.393	0.7085	0.123(1)	3.67(3)	19.8(16)
	3.856	0.6397	0.203(5)	2.40(7)	15.6(18)
	4.318	0.5535	0.326(6)	1.53(16)	9.51(10)
$Q^{*2}=4$	3.054	0.7939	0.026(3)	11.21(42)	23.3(31)
	3.642	0.7311	0.117(2)	4.06(14)	22.5(24)
	4.103	0.6596	0.196(2)	2.44(8)	18.4(21)
	4.600	0.5686	0.324(10)	1.71(10)	12.0(21)

Table I
Continued.

$L^*=0.4$	T^*	ρ^*	D^*	η^*	λ^*
$Q^{*2}=0$	1.893	0.5808	0.094(2)	2.51(20)	9.36(45)
	2.232	0.5365	0.147(1)	1.82(9)	8.90(36)
	2.536	0.4853	0.219(5)	1.32(9)	6.67(57)
	2.858	0.4185	0.326(3)	0.89(5)	4.92(47)
$Q^{*2}=1$	1.925	0.5879	0.084(1)	2.82(17)	10.12(60)
	2.239	0.5426	0.134(1)	2.03(7)	8.97(38)
	2.573	0.4913	0.206(1)	1.35(5)	7.39(55)
	2.869	0.4252	0.311(2)	0.92(8)	5.24(84)
$Q^{*2}=2$	1.999	0.6025	0.072(1)	3.36(11)	11.11(78)
	2.318	0.5555	0.121(1)	2.23(6)	9.58(33)
	2.663	0.5008	0.194(2)	1.53(8)	7.60(55)
	2.987	0.431	0.304(4)	0.97(5)	6.02(37)
$Q^{*2}=3$	2.096	0.6209	0.061(1)	3.98(14)	14.9(11)
	2.447	0.5717	0.109(1)	2.64(3)	10.52(82)
	2.794	0.5154	0.180(1)	1.71(7)	8.52(38)
	3.134	0.4428	0.290(5)	1.07(6)	6.37(56)
$Q^{*2}=4$	2.213	0.6396	0.051(6)	2.72(13)	14.04(71)
	2.599	0.5884	0.098(2)	2.95(7)	13.3(12)
	2.972	0.5307	0.168(1)	1.90(13)	10.51(17)
	3.350	0.4554	0.281(3)	1.21(4)	7.61(41)

Table I
Continued.

$L^*=0.505$	T^*	ρ^*	D^*	η^*	λ^*
$Q^{*2}=0$	1.638	0.5291	0.095(1)	2.02(6)	9.13(84)
	1.913	0.4891	0.141(2)	1.55(8)	7.62(42)
	2.190	0.4431	0.206(1)	1.10(6)	5.9(10)
	2.476	0.3835	0.305(1)	0.79(4)	4.43(18)
$Q^{*2}=1$	1.652	0.5349	0.083(1)	2.29(14)	9.97(74)
	1.924	0.4942	0.130(1)	1.67(6)	8.08(68)
	2.187	0.4474	0.193(1)	1.19(4)	6.48(18)
	2.509	0.3873	0.295(3)	0.81(5)	4.83(36)
$Q^{*2}=2$	1.728	0.5476	0.071(2)	2.80(10)	10.8(11)
	2.029	0.5049	0.118(1)	1.96(18)	8.70(92)
	2.288	0.4548	0.183(3)	1.34(13)	7.04(71)
	2.584	0.3926	0.283(1)	0.85(4)	4.93(40)
$Q^{*2}=3$	1.813	0.5643	0.058(1)	3.67(17)	11.5(14)
	2.102	0.5193	0.102(1)	2.40(13)	10.6(11)
	2.393	0.4691	0.166(2)	1.52(11)	7.49(65)
	2.692	0.4041	0.266(4)	0.95(10)	5.52(34)
$Q^{*2}=4$	1.922	0.5803	0.043(1)	5.28(74)	14.94(28)
	2.252	0.5335	0.092(2)	2.66(13)	11.39(60)
	2.541	0.4809	0.155(1)	1.71(10)	8.52(58)
	2.885	0.4135	0.259(3)	1.02(4)	5.80(24)

Table I
Continued.

$L^*=0.6$	T^*	ρ^*	D^*	η^*	λ^*
$Q^{*2}=0$	1.475	0.4900	0.094(1)	1.76(8)	9.39(96)
	1.726	0.4521	0.140(1)	1.37(8)	7.67(37)
	1.948	0.4088	0.199(2)	1.02(6)	6.00(68)
	2.211	0.3520	0.294(3)	0.66(6)	4.13(45)
$Q^{*2}=1$	1.490	0.4947	0.084(1)	2.01(8)	8.92(39)
	1.731	0.4563	0.128(1)	1.45(8)	7.46(59)
	2.011	0.4116	0.193(2)	1.10(4)	6.09(37)
	2.233	0.3519	0.287(1)	0.70(3)	3.85(27)
$Q^{*2}=2$	1.552	0.5083	0.069(1)	2.42(11)	10.06(31)
	1.810	0.4682	0.112(1)	1.72(9)	8.07(74)
	2.080	0.4214	0.177(2)	1.19(14)	6.09(35)
	2.314	0.3622	0.268(1)	0.79(4)	3.6(11)
$Q^{*2}=3$	1.610	0.5239	0.055(1)	3.04(26)	11.25(61)
	1.879	0.4819	0.096(1)	2.05(6)	9.40(67)
	2.137	0.4349	0.156(1)	1.38(9)	6.95(67)
	2.435	0.3758	0.250(3)	0.90(4)	4.97(38)
$Q^{*2}=4$	1.725	0.5381	0.040(1)	4.84(23)	10.0(24)
	2.023	0.4944	0.087(1)	2.37(6)	10.23(71)
	2.284	0.4452	0.147(2)	1.52(5)	7.85(70)
	2.608	0.3812	0.248(1)	0.99(7)	5.72(25)

Table I
Continued.

$L^*=0.8$	T^*	ρ^*	D^*	η^*	λ^*
$Q^{*2}=0$	1.234	0.4302	0.085(1)	1.51(5)	7.38(51)
	1.426	0.3956	0.126(1)	1.13(4)	6.21(28)
	1.632	0.3568	0.181(1)	0.85(2)	4.93(13)
	1.856	0.3051	0.267(3)	0.58(5)	3.64(23)
$Q^{*2}=1$	1.246	0.4364	0.074(1)	1.69(1)	8.09(50)
	1.458	0.4016	0.115(1)	1.23(7)	6.86(51)
	1.686	0.3602	0.173(1)	0.89(8)	5.56(41)
	1.885	0.3059	0.259(1)	0.60(4)	3.64(30)
$Q^{*2}=2$	1.308	0.4513	0.060(1)	2.23(6)	9.52(13)
	1.514	0.4143	0.099(2)	1.46(8)	7.22(22)
	1.712	0.3734	0.150(2)	1.02(3)	5.74(9)
	1.933	0.3207	0.233(1)	0.70(2)	4.04(24)
$Q^{*2}=3$	1.352	0.4666	0.047(1)	2.91(12)	9.02(12)
	1.579	0.4290	0.082(3)	1.85(5)	7.42(29)
	1.801	0.3858	0.136(2)	1.24(6)	6.19(40)
	2.045	0.3319	0.219(1)	0.78(6)	4.42(35)
$Q^{*2}=4$	1.447	0.4800	0.032(1)	4.92(47)	10.81(15)
	1.674	0.4416	0.073(1)	2.18(7)	8.87(40)
	1.914	0.3975	0.125(2)	1.42(1)	7.22(39)
	2.187	0.3402	0.212(1)	0.90(5)	4.65(41)

List of Figures

- 1 Phase diagrams for two selected elongated 2CLJQ fluids ($L^*=0.2$) where one is non-polar and the other strongly quadrupolar. Saturated densities, taken from [19], are represented by the lines joining at the critical point depicted by \bullet . The investigated state points are indicated by \circ for $Q^{*2}=0$ and by \triangle for $Q^{*2}=4$. 32
- 2 Phase diagrams for two selected quadrupolar 2CLJQ fluids ($Q^{*2}=1$) where one is spherical and the other strongly elongated. Saturated densities, taken from [19], are represented by the lines joining at the critical point indicated by \bullet . The investigated state points are indicated by \circ for $L^*=0$ and by \triangle for $L^*=0.8$. 33
- 3 Autocorrelation functions (ACF) for self-diffusion coefficient, shear viscosity, and thermal conductivity for the 2CLJQ fluid with $L^*=0.2$ and $Q^{*2}=1$ at $T^*=3.0295$ and $\rho^*=0.6573$. The vertical line denotes $t^*=0.1$. At this time all normalized autocorrelation functions have decayed to much less than $1/e$ denoted by the horizontal lines. 34
- 4 Normalized integrals of autocorrelation functions, i.e. self-diffusion coefficient, shear viscosity, and thermal conductivity. 35

- 5 Self-diffusion coefficient of spherical ($L^*=0$, empty symbols), elongated ($L^*=0.505$, grey symbols), and strongly elongated ($L^*=0.8$, full symbols) 2CLJQ fluids over reduced density along bubble lines. Reduced temperatures vary from $T_R=0.6$ to 0.9. Lines are guides for the eye. 36
- 6 Self-diffusion coefficient of spherical ($L^*=0$, empty symbols), elongated ($L^*=0.505$, grey symbols), and strongly elongated ($L^*=0.8$, full symbols) 2CLJQ fluids over number density along bubble lines. Reduced temperatures vary from $T_R=0.6$ to 0.9. Lines are guides for the eye. 37
- 7 Self-diffusion coefficient of spherical ($L^*=0$, empty symbols), elongated ($L^*=0.505$, grey symbols), and strongly elongated ($L^*=0.8$, full symbols) 2CLJQ fluids over number density in the homogeneous liquid at $T_R=0.9$. Lines are guides for the eye. 38
- 8 Self-diffusion coefficient of spherical ($L^*=0$, empty symbols) and strongly elongated ($L^*=0.8$, full symbols) 2CLJQ fluids over reduced temperature in the homogeneous liquid along different isochores. \circ : $\rho^*=0.8062$, \triangle : $\rho^*=0.8483$, \diamond : $\rho^*=0.9143$, \bullet : $\rho^*=0.4302$, \blacktriangle : $\rho^*=0.4513$, \blacklozenge : $\rho^*=0.4800$. Lines are guides for the eye. 39

- 9 Shear viscosity of spherical ($L^*=0$, empty symbols), elongated ($L^*=0.505$, grey symbols), and strongly elongated ($L^*=0.8$, full symbols) 2CLJQ fluids over number density along bubble lines. Reduced temperatures vary from $T_R=0.6$ to 0.9. Lines are guides for the eye. 40
- 10 Shear viscosity of spherical ($L^*=0$, empty symbols), elongated ($L^*=0.505$, grey symbols), and strongly elongated ($L^*=0.8$, full symbols) 2CLJQ fluids over number density in the homogeneous liquid at $T_R=0.9$. Lines are guides for the eye. 41
- 11 Shear viscosity of spherical ($L^*=0$, empty symbols) and strongly elongated ($L^*=0.8$, full symbols) 2CLJQ fluids over reduced temperature in the homogeneous liquid along different isochores. \circ : $\rho^*=0.8062$, \triangle : $\rho^*=0.8483$, \diamond : $\rho^*=0.9143$, \bullet : $\rho^*=0.4302$, \blacktriangle : $\rho^*=0.4513$, \blacklozenge : $\rho^*=0.4800$. Lines are guides for the eye. 42
- 12 Thermal conductivity of spherical ($L^*=0$, empty symbols), elongated ($L^*=0.505$, grey symbols), and strongly elongated ($L^*=0.8$, full symbols) 2CLJQ fluids over number density along bubble lines. Reduced temperatures vary from $T_R=0.6$ to 0.9. Lines are guides for the eye. 43

- 13 Thermal conductivity of spherical ($L^*=0$, empty symbols), elongated ($L^*=0.505$, grey symbols), and strongly elongated ($L^*=0.8$, full symbols) 2CLJQ fluids over number density in the homogeneous liquid at $T_R=0.9$. Lines are guides for the eye. 44
- 14 Thermal conductivity of spherical ($L^*=0$, empty symbols) and strongly elongated ($L^*=0.8$, full symbols) 2CLJQ fluids over reduced temperature in the homogeneous liquid along different isochores. \circ : $\rho^*=0.8062$, \triangle : $\rho^*=0.8483$, \diamond : $\rho^*=0.9143$, \bullet : $\rho^*=0.4302$, \blacktriangle : $\rho^*=0.4513$, \blacklozenge : $\rho^*=0.4800$. Lines are guides for the eye. 45

Fig. 1.

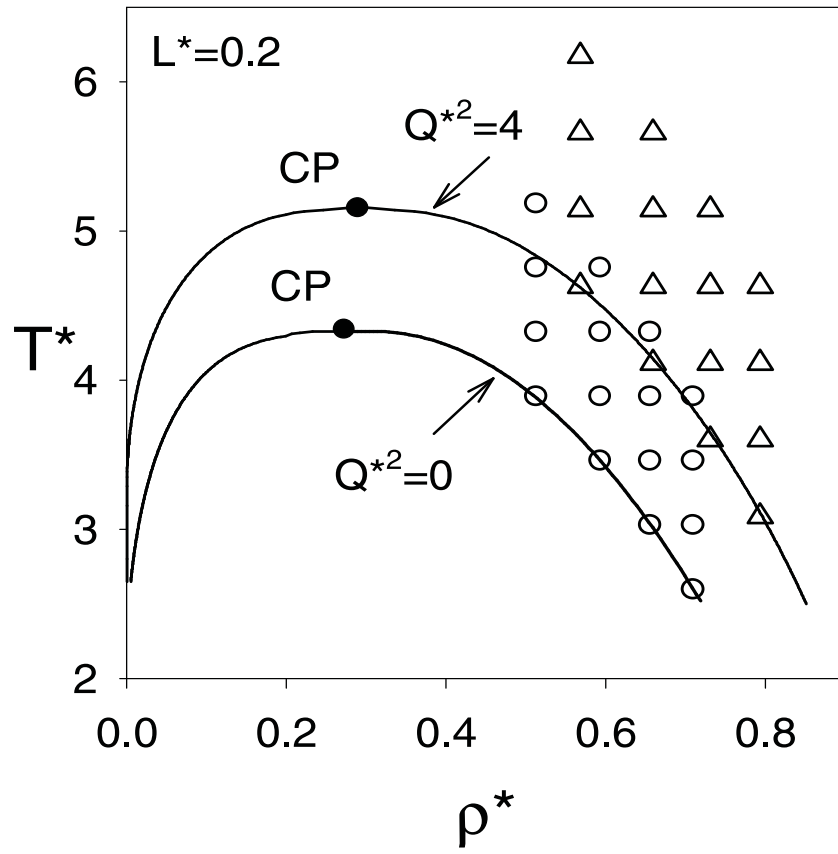


Fig. 2.

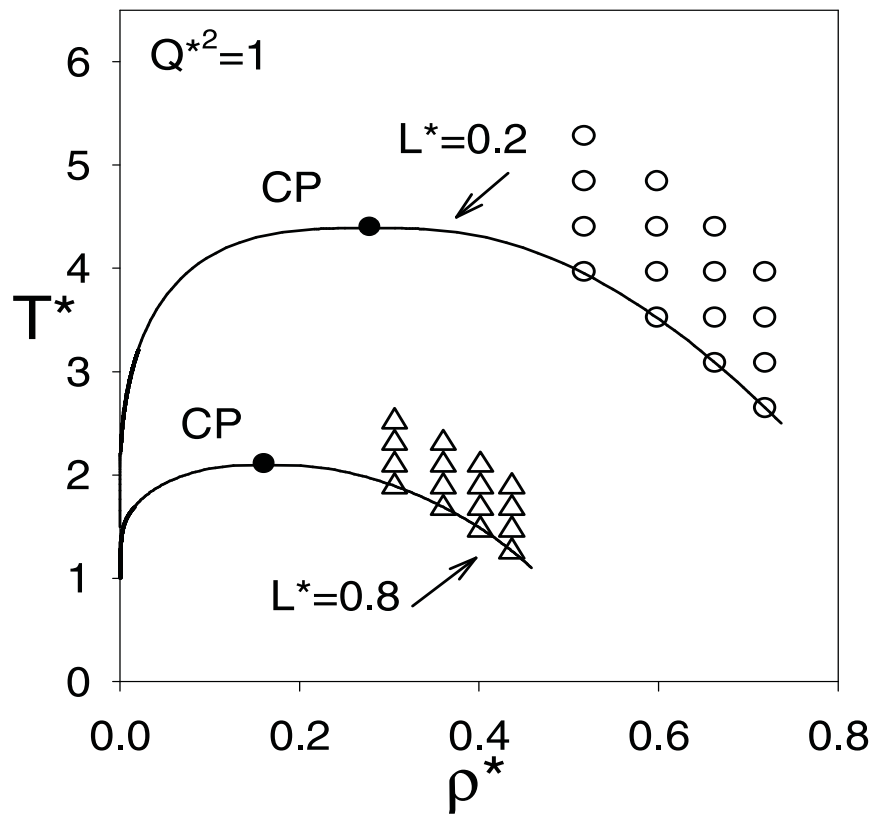


Fig. 3.

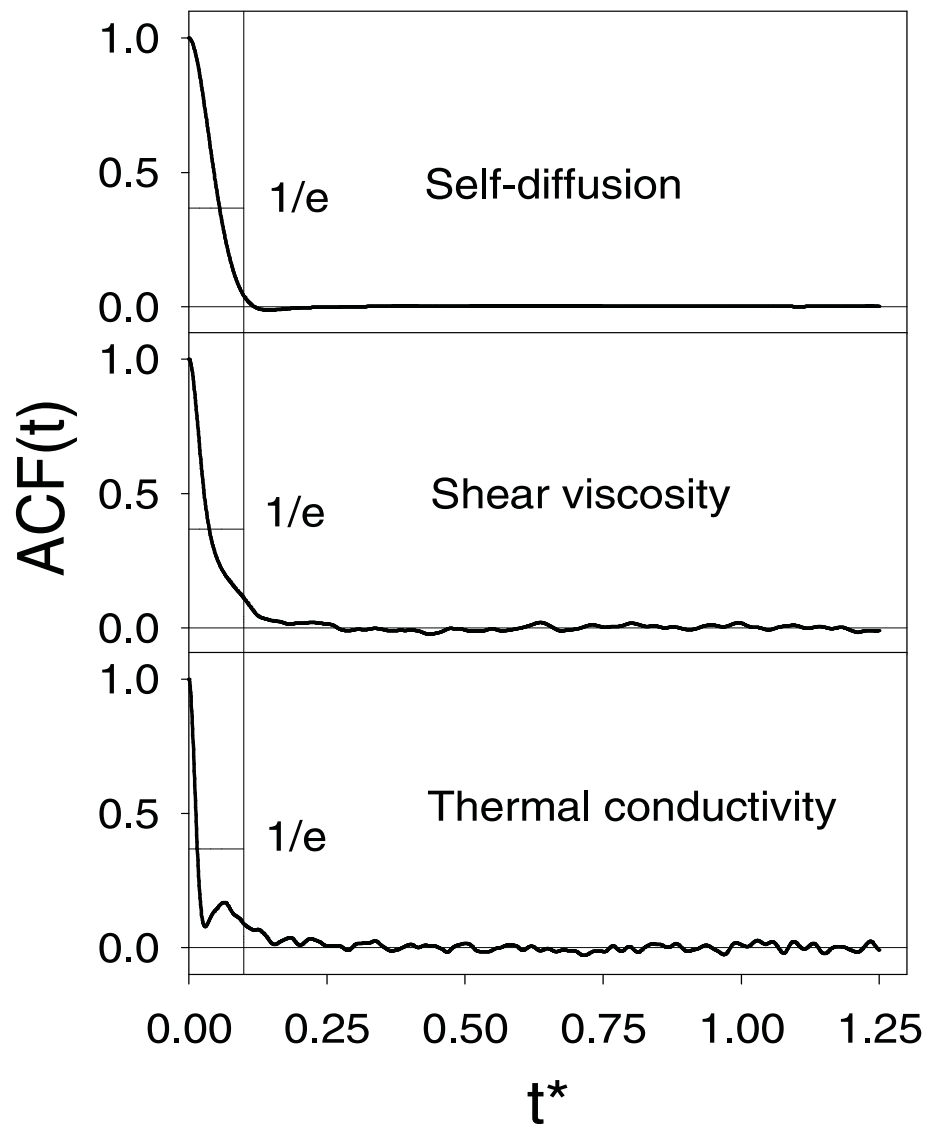


Fig. 4.

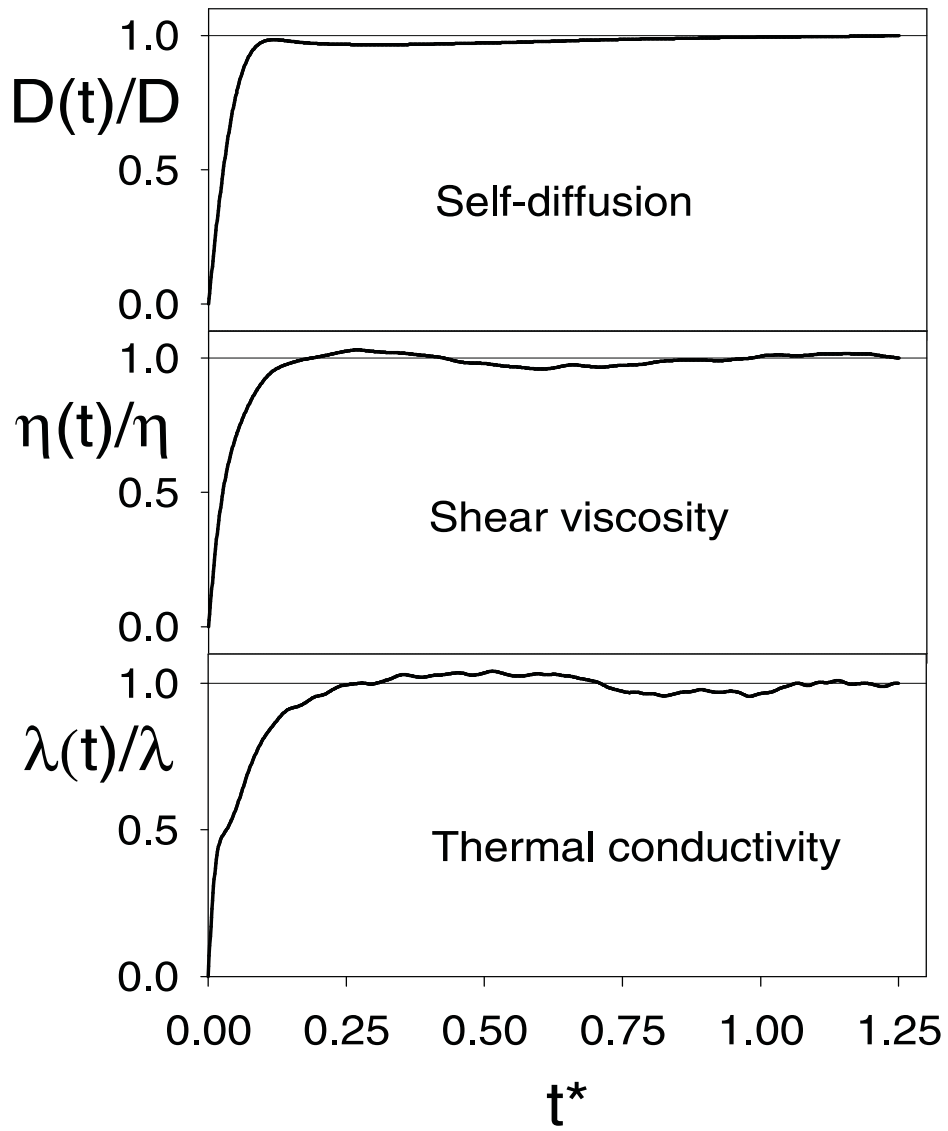


Fig. 5.

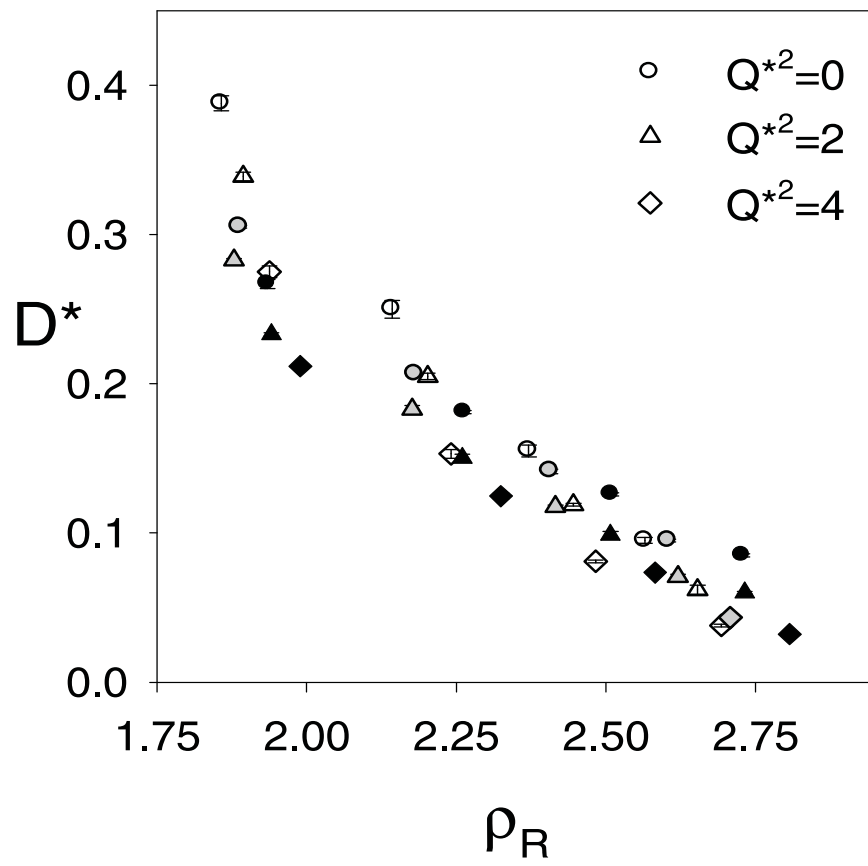


Fig. 6.

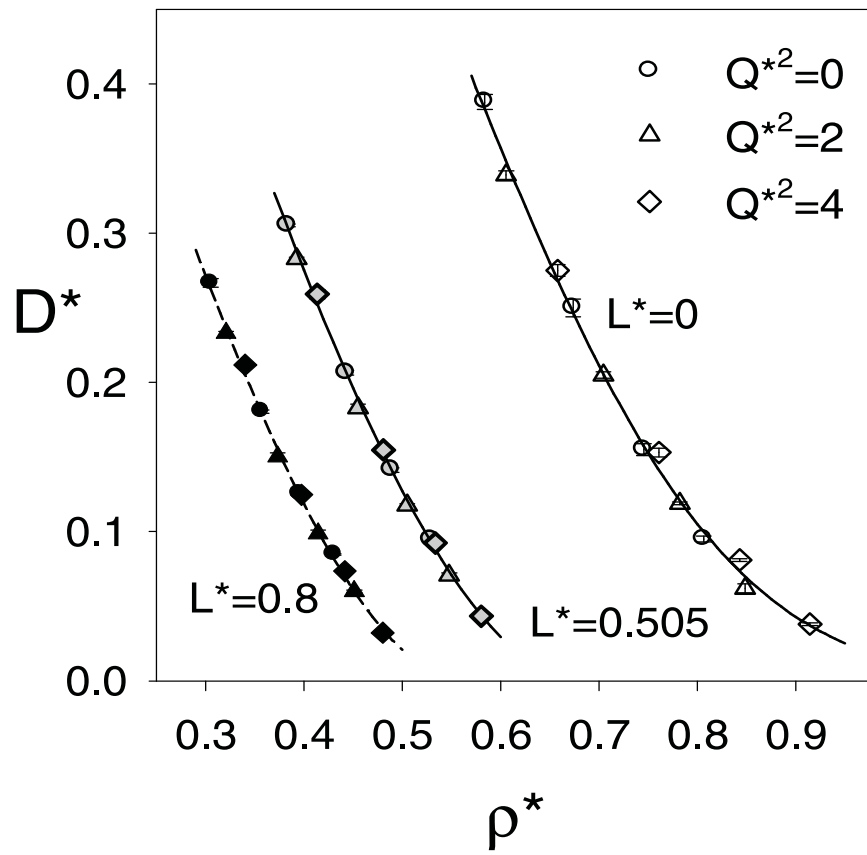


Fig. 7.

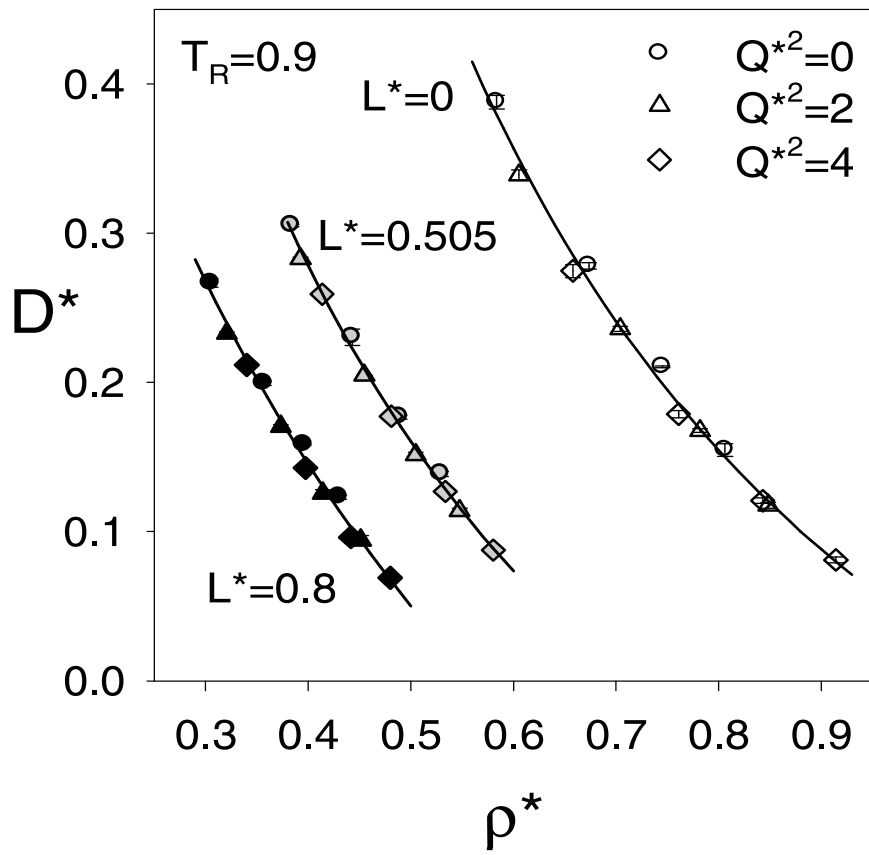


Fig. 8.

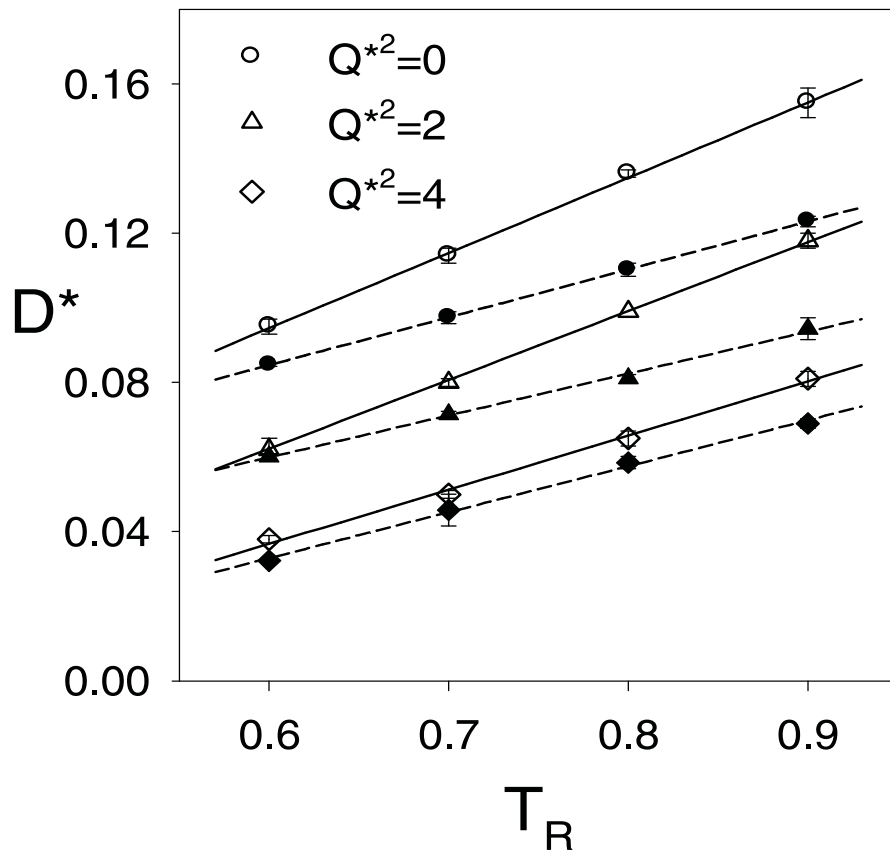


Fig. 9.

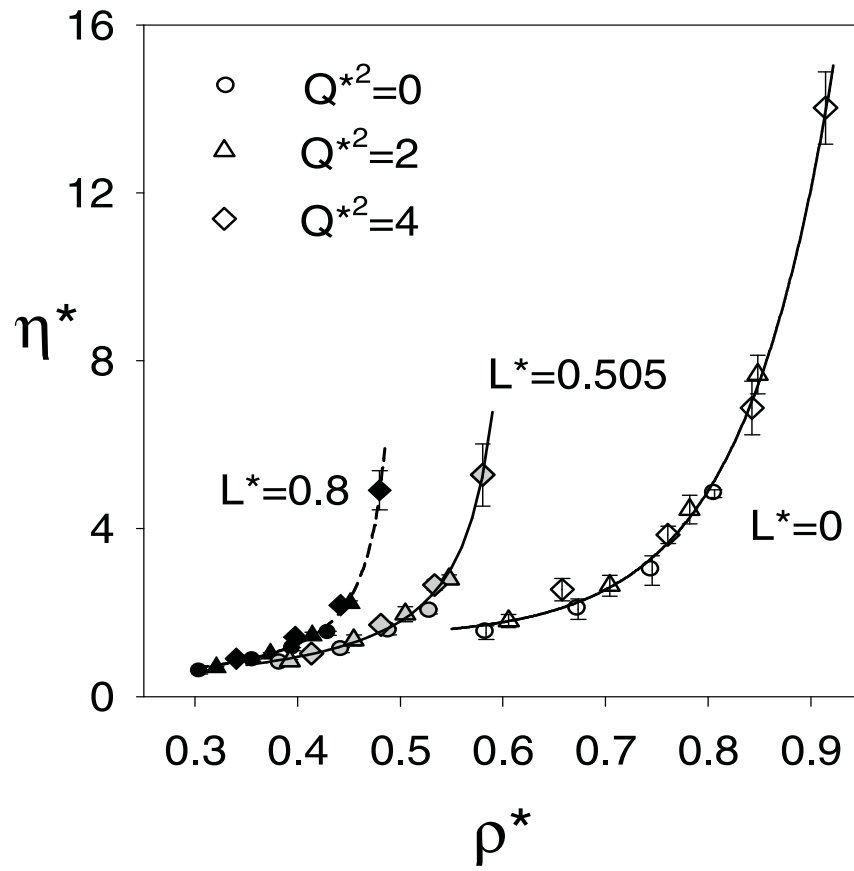


Fig. 10.

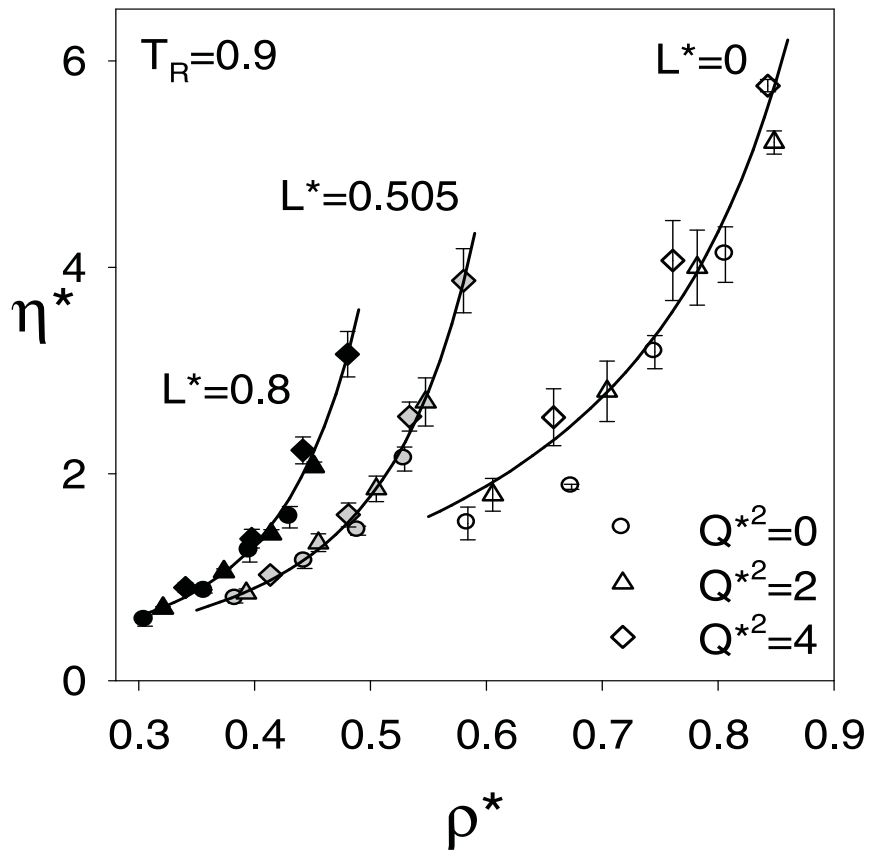


Fig. 11.

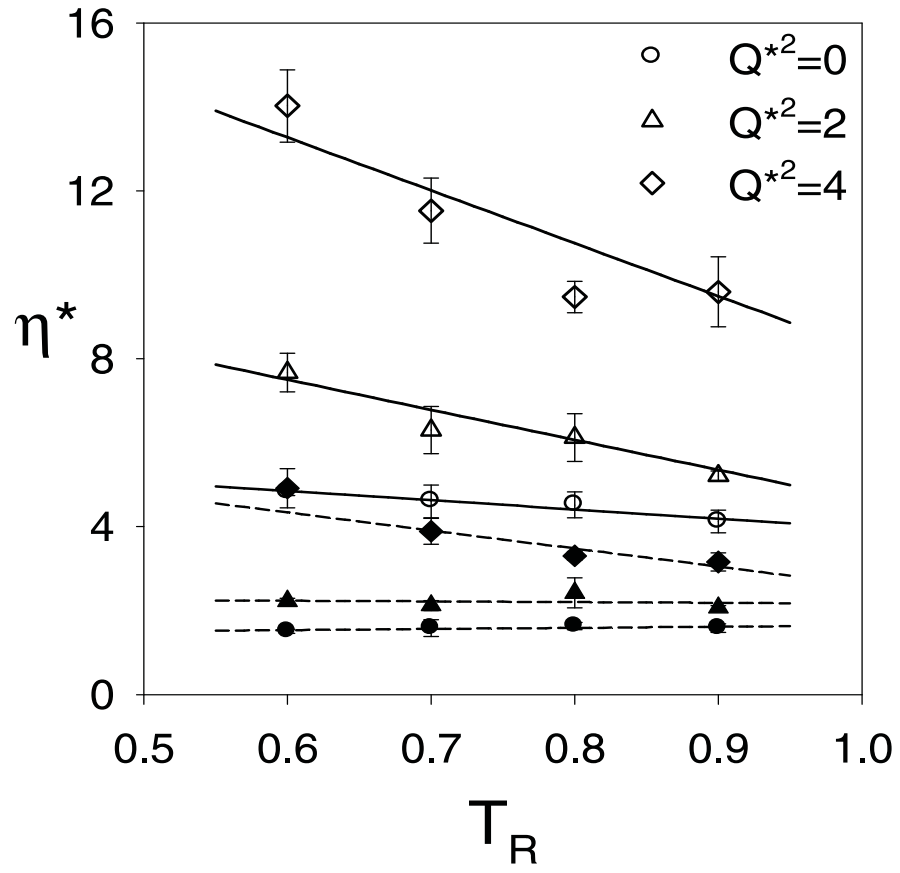


Fig. 12.

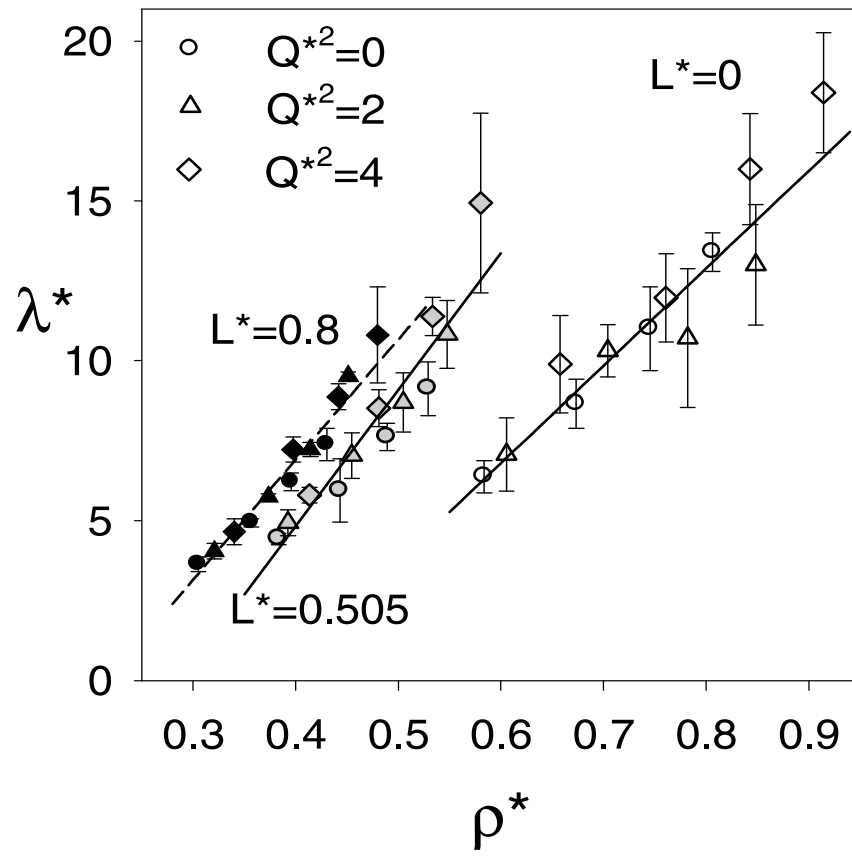


Fig. 13.

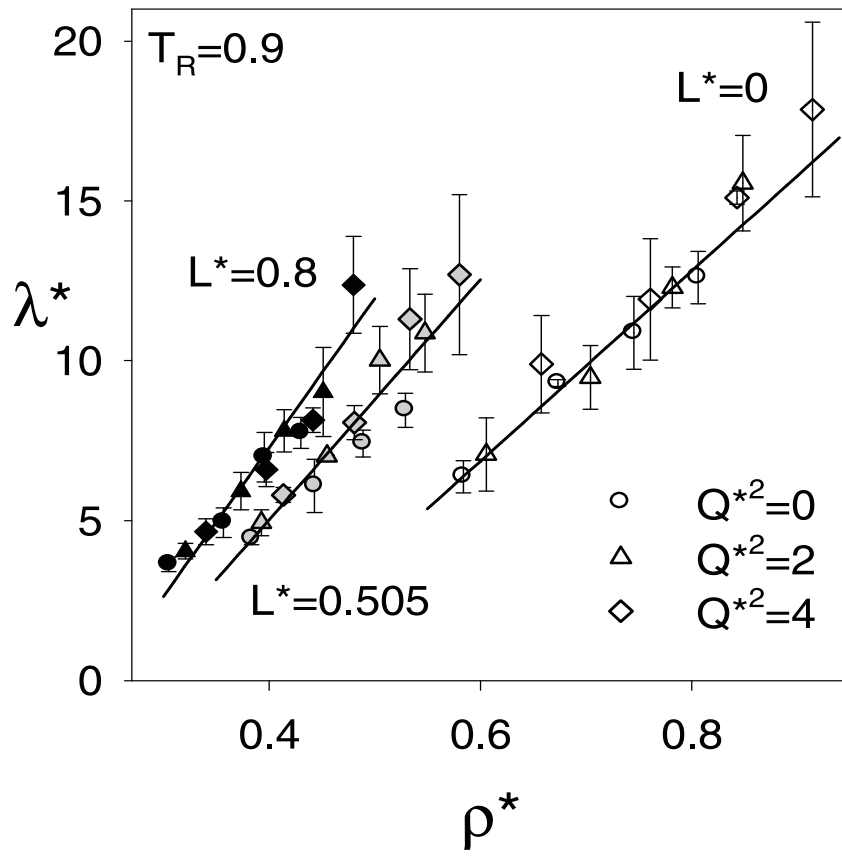


Fig. 14.

